INTERNATIONAL JOURNAL FOR NUMERICAL METHODS IN FLUIDS, VOL. 25, 679–695 (1997)

SPURIOUS VELOCITIES IN THE STEADY FLOW OF AN INCOMPRESSIBLE FLUID SUBJECTED TO EXTERNAL FORCES

J.-F. GERBEAU,[1] C. LE BRIS[1] AND M. BERCOVIER[2]*

[1] *ENPC-CERMICS, La Courtine, F- 93167 Noisy-Le-Grand Cedex, France*
[2] *The Hebrew University of Jerusalem, Jerusalem, Israel*

SUMMARY

We show that a non-physical velocity may appear in the numerical computation of the flow of an incompressible fluid subjected to external forces. A distorted mesh and the use of a numerical method which does not rigorously ensure the incompressibility condition turn out to be responsible for this phenomenon. We illustrate it with numerical examples and we propose a projection method which improves the results. © 1997 John Wiley & Sons, Ltd.

Int. J. Numer. Meth. Fluids, **25**: 679–695 (1997)

No. of Figures: 10. No. of Tables: 6. No. of References: 4.

KEY WORDS: incompressible flow; body force; projection method

1. INTRODUCTION

We are interested here in the steady state of an incompressible homogeneous fluid in the presence of a body force. This force may result from a coupling (e.g. magnetohydrodynamic equations or Boussinesq equations) or may be a given external force. For the sake of simplicity we shall only consider here the latter case.

When this force is the gradient of a potential, namely $\mathbf{f} = \nabla\Phi$, and when the velocity obeys the no-slip condition on the boundary of a fixed domain, we expect to obtain a fluid everywhere at rest. However, as will be seen, numerical simulations which do not ensure rigorously $div\ \mathbf{u} = 0$ may lead to a non-zero velocity.

We give a few examples of this phenomenon in Section 2 and we propose a first explanation in Section 3. The deformation of the mesh plays a role in the observed inaccuracies, but it is not their unique cause.

With a general force ($\mathbf{f} = \text{curl}\ g + \nabla\Phi$) we have noticed that the 'gradient part' may also produce a velocity field which pollutes the physical flow. We give an example of this in Section 2.4. For practical applications it is worth noticing that this phenomenon may *a fortiori* induce important numerical errors in coupled problems.

Section 4 is devoted to a projection method which eliminates the spurious speeds when $\mathbf{f} = \nabla\Phi$ (this method can easily be extended to the case of a force $\mathbf{f} = \nabla\Phi + \text{curl}\ g$ when Φ is *a priori* known). In Section 5 we extend this method in order to reduce the inaccuracy for any $\mathbf{f}$ whose decomposition is not *a priori* known.

* Correspondence to: M. Bercovier, The Hebrew University of Jerusalem, Jerusalem, Israel

Contract grant sponsor: PECHINEY

CCC 0271–2091/97/060679–17 $17.50

Received 28 June 1996
Revised 19 November 1996

Let us note that a method close to ours has already been suggested by Besson *et al.*[1] for a penalty formulation for the pressure. Nevertheless, our presentation allows us to establish a link between the spurious speeds and the deformation of the grid (see Appendix I). More precisely, we explain why spurious speeds do not appear on a right mesh with some particular forces and we also show that they do appear with some forces even on a right mesh. Moreover, we give an error estimate (see Appendix II) which proves that our method improves the results on any meshes.

The numerical simulations are performed with the FEM code FIDAP* Version 7.52 and with a home-made code. We use the pairs Q1/P0 and Q2/P1 of finite element spaces to approximate the velocity and the pressure. It is well-known that the pair Q1/P0 does not rigorously satisfy the Ladyzenskaia–Babuska–Brezzi condition and yields a spurious pressure (see e.g. References 2 and 3). Nevertheless, the problem presented here is independent of this fact and occurs also with the elements Q2/P1 which satisfy the LBB condition.

2. SOME NUMERICAL EXPERIMENTS

2.1. A free surface problem

Our initial motivation was to improve a 2D free surface algorithm. Two incompressible fluids separated by an interface are subjected to a force $\mathbf{f} = \nabla\Phi_0$, with $\Phi_0(x, y) = \frac{5}{2}y^2 - 10x$. Their densities are 2300 and 2150 kg m^{-3} and their viscosities 1·1 and 2·5 $m^2\ s^{-1}$. We solve the Navier–Stokes equations in a box with homogeneous Dirichlet boundary conditions on three sides and $\mathbf{u}\cdot\mathbf{n} = 0$ on the fourth side. The steady state interface is a curve $\Phi(x, y) = C$, where C is a constant determined by the conservation of volume. The theoretical velocity is zero. Numerically, the position of the interface is good, but we notice the appearance of a vortex (0·2 m s^{-1}) in each fluid (Figure 1).

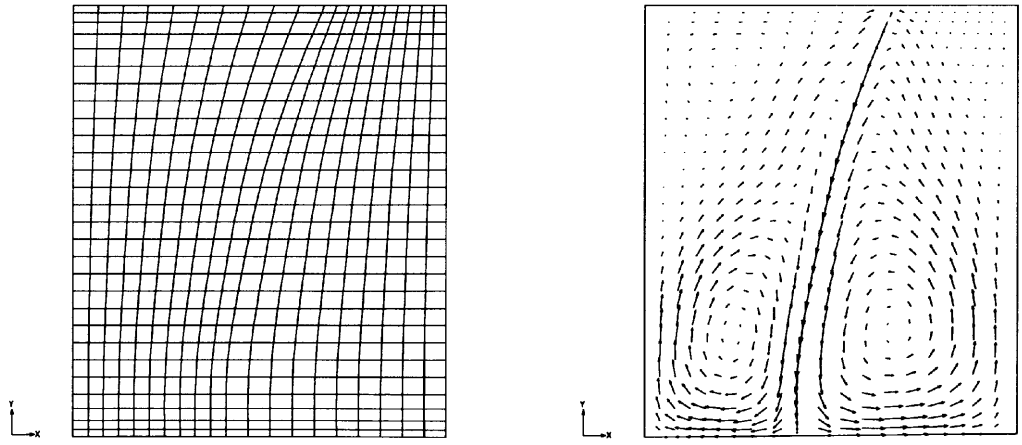

Figure 1. Spurious velocity (0·2 m s^{-1}) in two immiscible fluids submitted to $\mathbf{f} = \nabla\Phi_0$, with $\Phi_0(x, y) = \frac{5}{2}y^2 - 10x$: left, mesh; right, velocity field. This test is performed with FIDAP V7.52 with the Q1/P0 pair of finite elements

* FIDAP is a trademark of Fluid Dynamics International, Inc.

In order to understand the problem raised above, we simplify the experiment: in the following three tests we just consider a single fluid in a closed box Ω with various given forces and we solve the linear Stokes equations

$$-\eta\Delta\mathbf{u} + \nabla p = \rho\mathbf{f} \quad \text{on } \Omega, \tag{1}$$

$$\operatorname{div}\mathbf{u} = 0 \quad \text{on } \Omega, \tag{2}$$

$$\mathbf{u} = 0 \quad \text{on } \partial\Omega. \tag{3}$$

We set $\eta = 0{\cdot}01$ m^2 s^{-1} and $\rho = 1$ kg m^{-3} in the sequel.

2.2. *A fluid subjected to a constant force* $\mathbf{f}$

We assume $\mathbf{f}$ is constant and equal to (100, 100) on Ω. In Figure 2 we use Q1/P0 elements and we see that no velocity appears on a right grid (maximum about $0{\cdot}1 \times 10^{-11}$ m s^{-1}), whereas the velocity reaches 0·83 m s^{-1} on bent elements. In Figure 3 very similar results are obtained with Q2/P1 elements.

This suggests that the deformation of the grid plays a role in the inaccuracy on the velocity and may explain the difficulty mentioned in Section 2.1 in the case of a free surface (where elements are bent, since the mesh follows the interface in our computation).

2.3. *A fluid subjected to a force* $\mathbf{f} = \nabla\Phi$

In this test we use Q1/P0 elements and the force $\mathbf{f}$ is equal to $\nabla\Phi_1$, with $\Phi_1(x, y) = x^5 + x^4y^3 + x^2y + y^4$. The right-hand side of Figure 4 shows that spurious speeds appear on a bent mesh (maximum $0{\cdot}19 \times 10^{-1}$ m s^{-1}) but one may see on the left-hand side that they also appear on a grid whose elements are squares (maximum $0{\cdot}76 \times 10^{-3}$ m s^{-1}). Therefore the deformation of the mesh clearly makes worse the accuracy on the velocity, but imprecise results may also appear on rectangular elements.

Similar results were obtained with Q2/P1 elements.

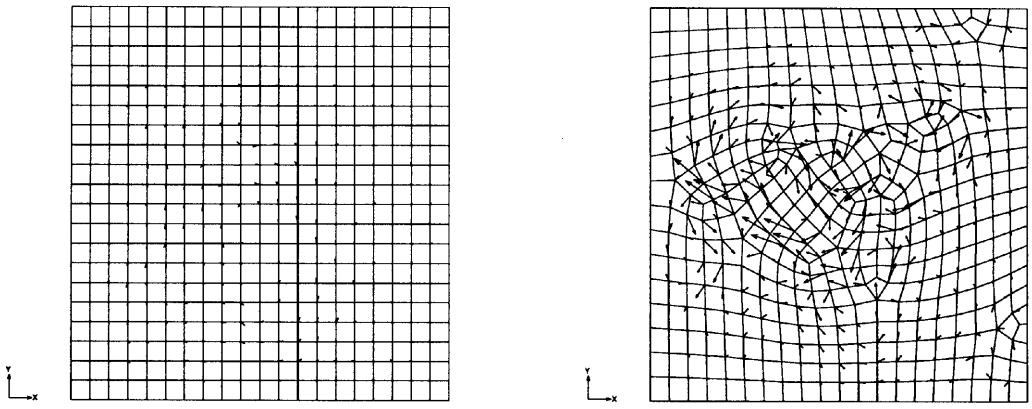

Figure 2. Fluid in presence of constant force with Q1/P0 elements. The influence of the shape of the mesh is striking: left, maximum speed $0{\cdot}1 \times 10^{-11}$ m s^{-1}; right, 0·83 m s^{-1}

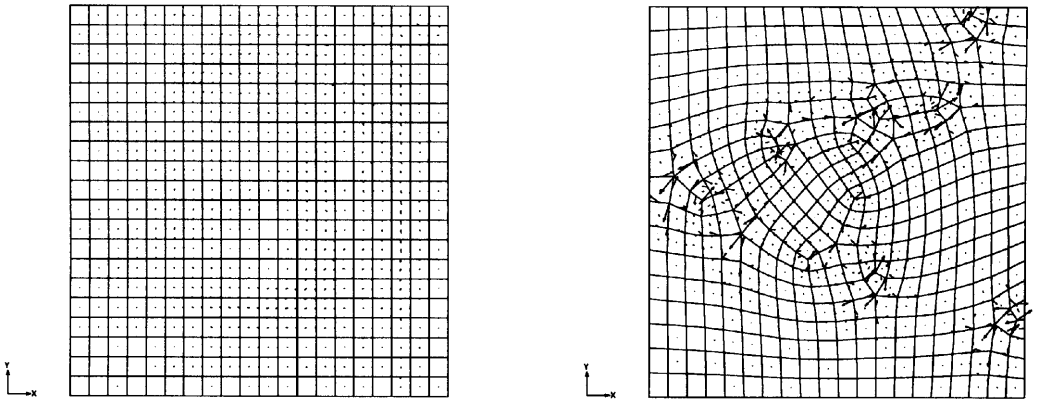

Figure 3. Same test as in Figure 2 but with Q2/P1 elements: left, maximum speed $0{\cdot}2 \times 10^{-11}$ m s^{-1}; right, $0{\cdot}3$ m s^{-1}

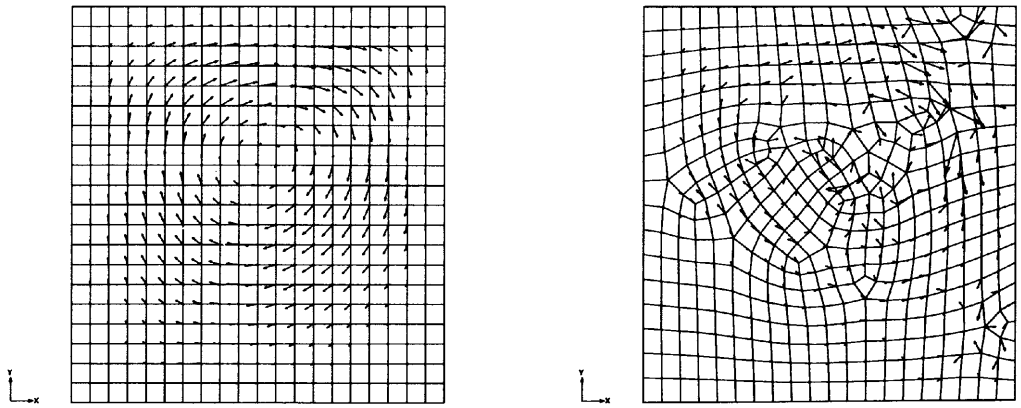

Figure 4. Fluid in presence of $\mathbf{f} = \nabla\Phi_1$: rectangular mesh, maximum speed $0{\cdot}76 \times 10^{-3}$ m s^{-1}; bent mesh, $0{\cdot}19 \times 10^{-1}$ m s^{-1}. This case is presented with the Q1/P0 pair of finite elements. We obtain similar results with Q2/P1 elements

2.4. *A fluid subjected to a force* $\mathbf{f} = \nabla\Phi + \text{curl } g$

The two previous tests deal with a fluid at rest. We now build an experiment where the force is the sum of a gradient part and a solenoidal part, thereby creating a non-zero velocity:

$$\mathbf{f} = \nabla\Phi + \text{curl } g. \tag{4}$$

In order to enforce the incompressibility and the no-slip condition on the boundary, we set $g = g_0$, with g_0 built as follows:

$$A = k[xy(H - x)(W - y)]^2, \tag{5}$$

$$\mathbf{u} = \text{curl } A, \tag{6}$$

$$g_0 = \text{curl } \mathbf{u}, \tag{7}$$

where H and W are respectively the height and the width of the 2D box and k is a constant. For the numerical computations, $H = W = 1$, $k = 0{\cdot}1$ and $\Phi(x, y) = \Phi_0(x, y) = \frac{5}{2}y^2 - 10x$.

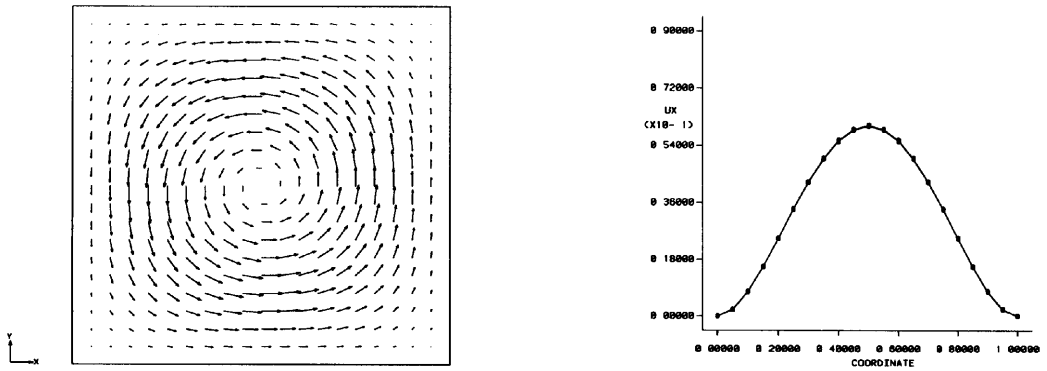

Figure 5. Fluid in presence of $\mathbf{f} = \nabla\Phi_0 + \operatorname{curl} g_0$ on *rectangular* elements: left, velocity field; right, comparison between theoretical first component of velocity and numerical one on straight line $y = 0{\cdot}4$. Finite elements Q1/P0

Note that the velocity $\mathbf{u}$ can be analytically computed with (6) and $p = \Phi$ (up to an additive constant).

Figure 5 shows the velocity field on a mesh with rectangular elements (left-hand side) and a comparison between the theoretical first component of the velocity and the numerical one on the straight line $y = 0{\cdot}4$ of Ω: the result is very precise (it is difficult to distinguish between the two curves). The same test computed on a distorted mesh is presented in Figure 6 with Q1/P0 elements and in Figure 7 with Q2/P1 elements: the flow is perturbed in both cases.

Remark 1

It is worth noticing that when $\Phi = 0$ (i.e. the force is divergence-free), the numerical velocity is very close to the theoretical one on both rectangular and bent elements. Thus the deformation of the grid seems to affect the velocity essentially in the presence of a non-divergence-free force.

2.5. *Other experiments*

Let us briefly mention other experiments which lead to analogous conclusions.

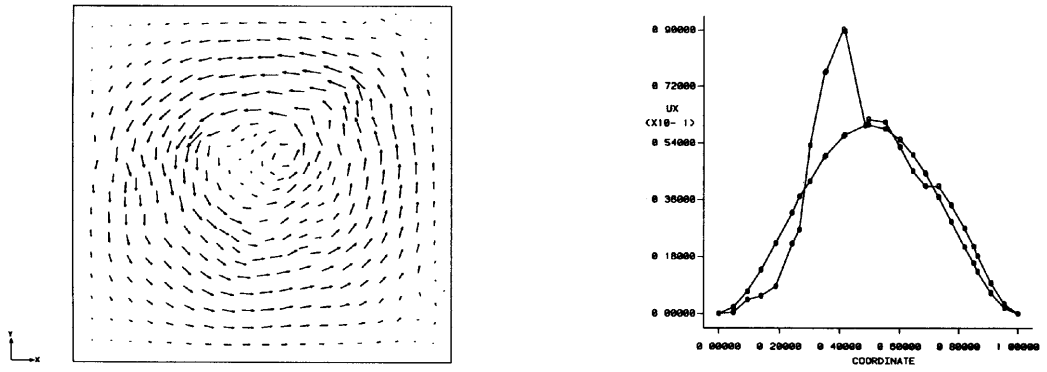

Figure 6. Same situation as on Figure 5 but on a *distorted* mesh

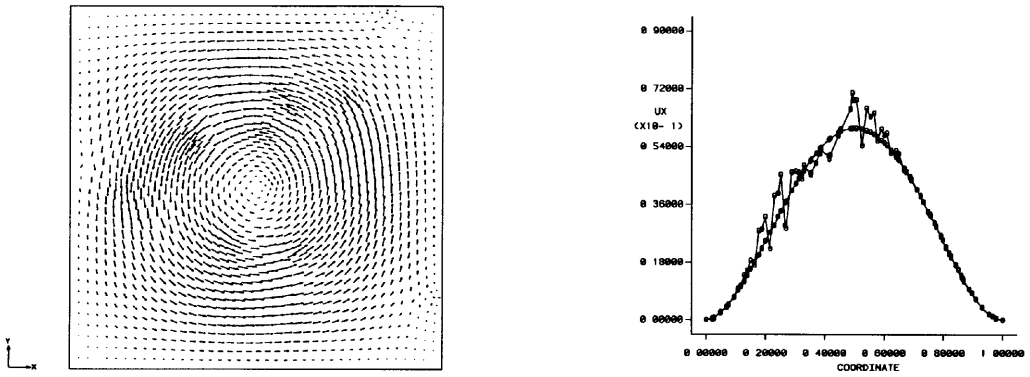

Figure 7. Same situation as in Figure 6 (distorted mesh) but with Q2/P1 elements. While the Q2/P1 approximation is better than Q1/P0, significant inaccuracies remain

The flow $\mathbf{u}$ defined by (6) is the solution of the Navier–Stokes equations for the force $\mathbf{f} = \nabla\Phi_0 + \text{curl}\, g_0 + \mathbf{u}\cdot\nabla\mathbf{u}$. If we compute the numerical solution in this non-linear setting, we observe that spurious velocities appear again on a bent mesh.

Likewise, they appear in many other experiments that we do not detail here and that involve other boundary conditions, a three-dimensional box, a transient flow, etc.

Let us also notice that the inaccuracy seems to increase with the Reynolds number and to decrease with the typical size of the mesh.

3. AN ATTEMPT AT EXPLANATION

Let us recall first of all why the fluid is at rest in the presence of $\mathbf{f} = \nabla\Phi$.

For $m \geqslant 0$ we denote as usual by $H^m(\Omega)$ the Sobolev space

$$H^m(\Omega) = \{u \in L^2(\Omega);\ D^\gamma u \in L^2(\Omega), \quad \forall\gamma,\ |\gamma| \leqslant m\},$$

where $\gamma = (\gamma_1, \gamma_2, \gamma_3)$ is a multi-index and $|\gamma| = \gamma_1 + \gamma_2 + \gamma_3$. For $m \geqslant 1$, $H_0^m(\Omega)$ is the subspace of $H^m(\Omega)$ consisting of functions vanishing on $\partial\Omega$. We denote by $L_0^2(\Omega)$ the space

$$L_0^2(\Omega) = \left\{q \in L^2(\Omega);\ \int_\Omega q\,\mathrm{d}x = 0\right\}.$$

We shall suppose in the sequel that $\mathbf{f} \in L^2(\Omega)^2$. The Stokes problem (1)–(3) may be formulated in a variational form: find $\mathbf{u} \in H_0^1(\Omega)^2$ and $p \in L_0^2(\Omega)$ such that

$$\begin{aligned} \eta\int_\Omega \nabla\mathbf{u}\cdot\nabla\mathbf{v}\,\mathrm{d}x - \int_\Omega p\,\mathrm{div}\,\mathbf{v}\,\mathrm{d}x &= \int_\Omega \mathbf{f}\cdot\mathbf{v}\,\mathrm{d}x, \\ \int_\Omega q\,\mathrm{div}\,\mathbf{u}\,\mathrm{d}x &= 0 \end{aligned} \tag{8}$$

for all $\mathbf{v} \in H_0^1(\Omega)^2$ and $q \in L_0^2(\Omega)$.

In particular, taking $\mathbf{v}=\mathbf{u}$, we have

$$\eta\int_\Omega |\nabla\mathbf{u}|^2 dx = \int_\Omega \mathbf{f}\cdot\mathbf{u} dx = \int_\Omega \nabla\Phi\cdot\mathbf{u} dx = -\int_\Omega \Phi \operatorname{div}\mathbf{u} dx = 0, \tag{9}$$

which shows that $\mathbf{u}=0$ almost everywhere in Ω, i.e. the fluid is at rest.

Let us notice that the crucial point of this proof is that $\operatorname{div}\mathbf{u}=0$ or, more precisely, that $\nabla\Phi$ is orthogonal (in $L^2(\Omega)$) to $\mathbf{u}$ as soon as $\operatorname{div}\mathbf{u}=0$ in Ω and $\mathbf{u}\cdot\mathbf{n}=0$ on $\partial\Omega$. As we recall hereafter, this property does not hold for the discrete problem.

Following the presentation of Girault and Raviart,[2] we introduce for each $h>0$ two finite-dimensional spaces W_h and Q_h such that $W_h \subset H^1(\Omega)^2$ and $Q_h(\Omega)\subset L^2(\Omega)$. The latter is assumed to contain the constant functions. We set

$$X_h = W_h \cap H_0^1(\Omega)^2 = \{\mathbf{v}_h \in W_h;\ \mathbf{v}_{h|\partial\Omega}=0\},$$
$$M_h = Q_h \cap L_0^2(\Omega) = \left\{q_h \in Q_h;\ \int_\Omega q_h dx = 0\right\}.$$

The variational problem (8) is then approximated by: find $u_h \in X_h$ and $p_h \in M_h$ such that

$$\eta\int_\Omega \nabla\mathbf{u}_h\cdot\nabla v_h dx - \int_\Omega P_h \operatorname{div} v_h dx = \int_\Omega f\cdot v_h dx \int_\Omega q_h \operatorname{div} u_h dx = 0, \tag{10}$$

for all $\mathbf{v}_h \in X_h$ and $q_h \in M_h$. In the case of $\mathbf{f}=\nabla\Phi$ we obtain, as in the continuous case,

$$\int_\Omega |\nabla\mathbf{u}_h|^2 dx = -\frac{1}{\eta}\int_\Omega \Phi \operatorname{div}\mathbf{u}_h dx, \tag{11}$$

but now the right-hand side of (11) is not necessarily zero since Φ does not belong to M_h in general. Thus the approximated velocity is not zero, which may explain the inaccuracies observed in the numerical computations of Sections 2.1–2.3. Moreover, equation (11) shows that the approximated velocity increases when the viscosity η decreases, which has been noticed in the experiments.

Let us note that the above considerations do not explain the influence of the grid. Distorted elements are known to produce inaccuracies,[4] but we are unfortunately not able to derive here a precise error estimate linking the spurious speeds with the deformation of the mesh.

Nevertheless, we propose now a way to avoid spurious velocities when $\mathbf{f}=\nabla\Phi$ which will enable us to understand why some results are much better on rectangular elements (at least with some potentials).

4. A METHOD TO AVOID SPURIOUS SPEEDS WHEN $\mathbf{f}=\nabla\Phi$

In the following developments we shall suppose, without loss of generality, that $\int_\Omega \Phi dx = 0$. The potentials Φ_0 and Φ_1 of the previous section can easily be changed to satisfy this property.

In order to obtain a zero velocity field when $\mathbf{f}=\nabla\Phi$, we suggest the following projection method.

First step

We compute $\Pi_h\Phi$, the orthogonal projection in $L^2(\Omega)$ of Φ onto M_h. In other words, we search $\Pi_h\Phi \in M_h$ such that

$$\int_\Omega \Pi_h\Phi q_h dx = \int_\Omega \Phi q_h dx \tag{12}$$

for all $\mathbf{v}_h \in X_h$ and $q_h \in M_h$.

Second step

We replace (10) by this alternative formulation of the Stokes problem: find $\mathbf{u}_h \in X_h$ and $p_h \in M_h$ such that

$$\begin{gathered} \eta \int_\Omega \nabla \mathbf{u}_h \cdot \nabla \mathbf{v}_h \mathrm{d}x - \int_\Omega p_h \operatorname{div} \mathbf{v}_h \mathrm{d}x = -\int \Pi_h \phi \operatorname{div} v_h \mathrm{d}x, \\ \int_\Omega q_h \operatorname{div} \mathbf{u}_h \mathrm{d}x\mathrm{d}y = 0 \end{gathered} \tag{13}$$

for all $\mathbf{v}_h \in X_h$ and $q_h \in M_h$.

Thus we have

$$\int_\Omega |\nabla \mathbf{u}_h|^2 \mathrm{d}x = -\frac{1}{\eta} \int_\Omega \Pi_h \Phi \operatorname{div} \mathbf{u}_h \mathrm{d}x = 0, \tag{14}$$

since $\Pi_h \Phi \in M_h$. Therefore $\mathbf{u}_h = 0$.

We have tested this method (with a home-made code) in the experiments of Sections 2.2 and 2.3: the spurious velocities disappear on both a rectangular and a distorted mesh (see Table I for Q1/P0 elements and Table II for Q2/P1 elements).

We are now able to explain why spurious speeds do not appear on rectangular elements with the potentials Φ_0 and Φ_1 of experiments 2.2 and 2.4, at least for the Q1/P0 pair of finite element spaces. For this purpose let us compare

$$\int_\Omega \mathbf{f} \cdot \mathbf{v}_j \mathrm{d}x = -\int_\Omega \Phi \operatorname{div} \mathbf{v}_j \mathrm{d}x$$

with

$$-\int_\Omega \Pi_h \Phi \operatorname{div} \mathbf{v}_j \mathrm{d}x,$$

where $\mathbf{v}_j$ denotes the velocity shape function (Q1) relative to node j. Let us consider the four elements T_k, $k = 1, \ldots, 4$, around node j (see Figure 10 in Appendix I). When the elements are *identical*

Table I. Maximum velocities (m s^{-1}) with classical method and projection method when $\mathbf{f} = \nabla\phi$ with Q1/P0 pair of finite elements

		Classical method	Projection method
Experiment 2.2	Rectangular elements	$0{\cdot}1 \times 10^{-11}$	$0{\cdot}08 \times 10^{-11}$
($\mathbf{f} = cste$)	Distorted elements	0·83	$0{\cdot}2 \times 10^{-11}$
Experiment 2.3	Rectangular elements	$0{\cdot}76 \times 10^{-3}$	$0{\cdot}7 \times 10^{-12}$
($\mathbf{f} = \nabla\phi_1$)	Distorted elements	$0{\cdot}17 \times 10^{-1}$	$0{\cdot}2 \times 10^{-12}$

Table II. Same case as in Table I but with Q2/P1 pair of finite elements

		Classical method	Projection method
Experiment 2.2	Rectangular elements	$0{\cdot}2 \times 10^{-11}$	$0{\cdot}2 \times 10^{-11}$
($\mathbf{f} = cste$)	Distorted elements	0·3	$0{\cdot}5 \times 10^{-8}$
Experiment 2.3	Rectangular elements	$0{\cdot}4 \times 10^{-3}$	$0{\cdot}1 \times 10^{-11}$
($\mathbf{f} = \nabla\phi_1$)	Distorted elements	$0{\cdot}14 \times 10^{-1}$	$0{\cdot}3 \times 10^{-10}$

rectangles whose sides are parallel to the co-ordinates axes, we establish in Appendix I that these two integrals are equal, for each j, whenever the following property holds:

$$\begin{aligned}\sum_{k=1}^{4}(-1)^k\int_{T_k}(x-x_k^c)\Phi(x,y)\mathrm{d}x\mathrm{d}y=0,\\ \sum_{k=1}^{4}(-1)^k\int_{T_k}(y-y_k^c)\Phi(x,y)\mathrm{d}x\mathrm{d}y=0,\end{aligned}\tag{15}$$

where (x_k^c, y_k^c) are the co-ordinates of the centre C_k of T_k.

In particular, (15) holds for any $\Phi(x, y)=\Psi_1(x)+\Psi_2(y)+\beta(x, y)$, where Ψ_1 and Ψ_2 denote two arbitrary functions and β is an arbitrary bilinear application.

Thus on rectangular elements, for potentials of the above form, it is equivalent to implement $\int_\Omega \mathbf{f}\cdot\mathbf{v}_j\mathrm{d}x$ or $-\int_\Omega \Pi_h\Phi\,\mathrm{div}\,\mathbf{v}_j\mathrm{d}x$ with Q1/P0 elements. Therefore in this particular case the traditional system (8) leads to the same calculus as system (13) (which yields zero velocities, as proved above). This explains the good results obtained on a rectangular mesh for a simple force like that in experiment 2.2. In contrast, the potential $\Phi_1(x, y)=x^5+x^4y^3+x^2y+y^4$ of experiment 2.3 does not satisfy (15) and we indeed check that it yields a wrong velocity even on rectangular elements.

In the case of gravity, no spurious speeds appear on a right grid with Q2/P1 elements, since the potential of the force belongs to the pressure space. Note that this is no longer true on a distorted mesh.

5. EXTENSION TO THE GENERAL CASE

The method presented in the previous section leads to very good results when $\mathbf{f}$ is the gradient of a known potential Φ. It can be straightforwardly extended to the case $\mathbf{f}=\nabla\Phi+\mathrm{curl}\,g$ when Φ and g are given.

The purpose of this last section is to extend this method to treat the case of any force $\mathbf{f}$ whose decomposition into a gradient and a solenoidal part is unknown.

First step

Let Y_h be a finite-dimensional space such that $Y_h\subset H^1(\Omega)$ (in practice we can take $Y_h=X_h$). We solve the following problem in order to compute an approximated gradient part of $\mathbf{f}$: find $\Phi_h\in Y_h$ such that

$$\int_\Omega \nabla\Phi_h\cdot\nabla\psi_h\mathrm{d}x=\int_\Omega \mathbf{f}\cdot\nabla\psi_h\mathrm{d}x\tag{16}$$

for all $\psi_h\in Y_h$.

Second step

We compute $\Pi_h\Phi_h\in M_h$ such that

$$\int_\Omega \Pi_h\Phi_h q_h\mathrm{d}x=\int_\Omega \Phi_h q_h\mathrm{d}x\tag{17}$$

for all $q_h\in M_h$.

Third step

Finally we solve the Stokes problem as follows: find $\mathbf{u}_h \in X_h$ and $p \in M_h$ such that

$$\begin{aligned} \eta \int_\Omega \nabla \mathbf{u}_h \cdot \nabla \mathbf{v}_h \mathrm{d}x - \int_\Omega p_h \operatorname{div} \mathbf{v}_h \mathrm{d}x &= \int_\Omega (\mathbf{f} - \nabla \Phi_h) \cdot \mathbf{v}_h \mathrm{d}x - \int_\Omega \Pi_h \Phi_h \operatorname{div} \mathbf{v}_h \mathrm{d}x, \\ \int_\Omega q_h \operatorname{div} \mathbf{u}_h \mathrm{d}x &= 0 \end{aligned} \tag{18}$$

for all $\mathbf{v}_h \in X_h$ and $q_h \in M_h$.

Remark 2

Note that $Y_h \subset H^1(\Omega)$ (in practice Φ_h is approximated in the same space as the velocity), thus the calculus of $\nabla \Phi_h$ is consistent.

Remark 3

When $\operatorname{div} \mathbf{f} \in L^2(\Omega)$, the problem solved in the first step is the approximated variational formulation of

$$\begin{aligned} \Delta \Phi &= \operatorname{div} \mathbf{f} \quad \text{on } \Omega \\ \frac{\partial \Phi}{\partial \mathbf{n}} &= \mathbf{f} \cdot \mathbf{n} \quad \text{on } \partial\Omega. \end{aligned}$$

Let us check what happens when $\mathbf{f} = \nabla \Phi$. We recall that the method of Section 4 yields a zero velocity field. Unfortunately, that is not the case here. More precisely, we have

$$\int_\Omega |\nabla \mathbf{u}_h|^2 \mathrm{d}x = \frac{1}{\eta} \int_\Omega (\mathbf{f} - \nabla \Phi_h) \cdot \mathbf{u}_h \mathrm{d}x. \tag{19}$$

Nevertheless, we prove in Appendix II that this estimate is better than (11) and the numerical results show hereafter that this method actually improves the accuracy in experiments 2.2–2.4.

Tables III and IV show the results obtained when $\mathbf{f} = \nabla \Phi$ (but of course Φ is not *a priori* known) with Q1/P0 and Q2/P1 elements. Note that they are less precise than with the method of Section 4 (especially for experiment 2.3) but still better than with the classical method.

Figure 8 shows the results obtained with the force $\mathbf{f} = \operatorname{curl} g_0 + \nabla \Phi_0$ of experiment 2.4 on a distorted mesh (with g_0 and Φ_0 not *a priori* known by the code). Note that the computed velocity is very close to the theoretical one, whereas the classical method gives a very bad flow on the same mesh (Figures 6 and 7). As previously, elements Q2/P1 and Q1/P0 give similar results (though Q2/P1 is of course slightly better).

Tables V and VI show the dependence of $\|\mathbf{u}_h\|_{L^2(\Omega)^2}$ on h in the case $f = \nabla \phi_1$ on rectangular elements. In the case of Q1/P0 elements (resp. Q2/P1) the numerical experiment shows that when

Table III. Maximum velocities (m s^{-1}) with classical method and projection method for arbitrary $\mathbf{f}$ with Q1/P0 pair of finite elements

		Classical method	Projection method for arbitrary $\mathbf{f}$
Experiment 2.2	Rectangular elements	$0{\cdot}1 \times 10^{-11}$	$0{\cdot}1 \times 10^{-11}$
($\mathbf{f} = cste$)	Distorted elements	0·83	$0{\cdot}2 \times 10^{-11}$
Experiment 2.3	Rectangular elements	$0{\cdot}76 \times 10^{-3}$	$0{\cdot}19 \times 10^{-5}$
($\mathbf{f} = \nabla \phi_1$)	Distorted elements	$0{\cdot}17 \times 10^{-1}$	$0{\cdot}4 \times 10^{-3}$

Table IV. Same case as in Table III with Q2/P1 pair of finite elements

		Classical method	Projection method for arbitrary **f**
Experiment 2.2	Rectangular elements	$0{\cdot}9 \times 10^{-12}$	$0{\cdot}44 \times 10^{-11}$
($\mathbf{f} = cste$)	Distorted elements	0·3	$0{\cdot}14 \times 10^{-10}$
Experiment 2.3	Rectangular elements	$0{\cdot}4 \times 10^{-3}$	$0{\cdot}7 \times 10^{-7}$
($\mathbf{f} = \nabla\phi_1$)	Distorted elements	$0{\cdot}14 \times 10^{-1}$	$0{\cdot}25 \times 10^{-4}$

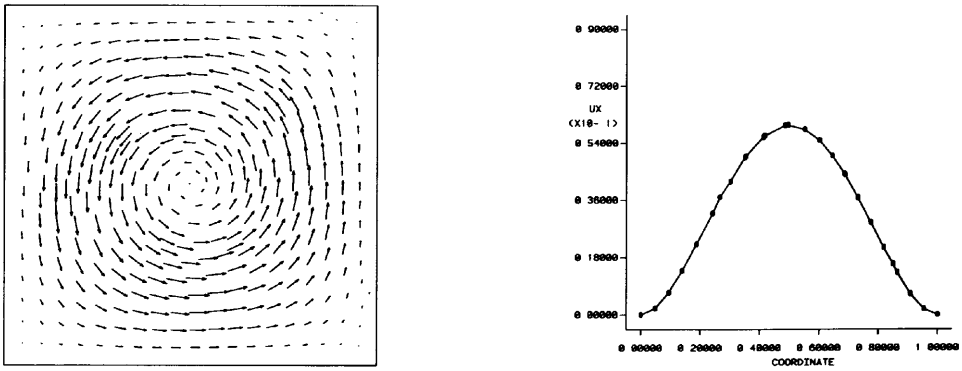

Figure 8. Projection method for experiment 2.4 on same distorted mesh as in Figure 6. Note that the theoretical curve and the numerical one are now the same. A very precise result is also obtained by the projection method with Q2/P1 elements in the case corresponding to Figure 7

Table V. Value of $\|\mathbf{u}_h\|_{L^2(\Omega)^2}$ when mesh step h decreases (case $\mathbf{f} = \nabla\phi_1$) with Q1/P0 elements

h	Classical method	Projection method
0·067	$6{\cdot}49 \times 10^{-4}$	$2{\cdot}7 \times 10^{-6}$
0·05	$3{\cdot}66 \times 10^{-4}$	$8{\cdot}6 \times 10^{-7}$
0·033	$1{\cdot}63 \times 10^{-4}$	$1{\cdot}7 \times 10^{-7}$
0·028	$1{\cdot}19 \times 10^{-4}$	$9{\cdot}2 \times 10^{-8}$

Table VI. Same case as in Table V but with Q2/P1 elements

h	Classical method	Projection method
0·083	$2{\cdot}1 \times 10^{-4}$	$1{\cdot}9 \times 10^{-7}$
0·067	$0{\cdot}86 \times 10^{-4}$	$5{\cdot}1 \times 10^{-8}$
0·05	$0{\cdot}28 \times 10^{-4}$	$0{\cdot}9 \times 10^{-8}$
0·045	$0{\cdot}19 \times 10^{-4}$	$0{\cdot}5 \times 10^{-8}$

the classical method is used, $\|\mathbf{u}_h\|_{L^2(\Omega)^2}$ decreases proportionally to h^2 (resp. h^4), whereas it decreases proportionally to h^4 (resp. h^6) with the projection method.

With an arbitrary potential Φ we show rigorously in Appendix II that with Q1/P0 elements, $\|\mathbf{u}_h\|_{L^2(\Omega)^2}$ decreases at least proportionally to h with the classical method and proportionally to h^2 with the projection method.

6. CONCLUSIONS

It has been shown that spurious speeds can appear in the flow of an incompressible fluid subjected to external forces if the numerical velocity is not rigorously divergence-free. We have proposed a method which completely cancels the spurious field for a force whose gradient part is *a priori* known and which improves the results when the gradient part is unknown. A mathematical study of the method has been presented. This method has been tested with Q1/P0 and Q2/P1 pairs of finite elements, but it can easily be extended to other pairs of elements.

We have also shown that no spurious field appears with a particular set of forces on a mesh composed of Q1/P0 rectangular elements. This explains the good results obtained on regular meshes with some simple forces such as gravity. Nevertheless, it has been shown that spurious speeds may still appear on a regular mesh. Moreover, as soon as the mesh is composed of distorted elements, very inaccurate results may occur even with gravity. In all these cases the method that we have proposed improves significantly the results.

ACKNOWLEDGEMENTS

This work was partially supported by PECHINEY, Direction des Recherches et Développements, France.

APPENDIX I

In this appendix we use the Q1/P0 pair of finite element spaces to approximate the velocity and the pressure.

I.1. Notation

We shall denote by T_{ref} the reference unit square $[0,\ 1] \times [0,\ 1]$ and by F_k the bilinear mapping that maps T_{ref} onto any quadrilateral T_k. F_k is defined by

$$F_k(\xi, \eta) = (x, y) = (A_0^k + A_1^k \xi + A_2^k \eta + A_3^k \xi\eta, B_0^k + B_1^k \xi + B_2^k \eta + B_3^k \xi\eta). \tag{20}$$

Denoting by (a_i^k, b_i^k) the co-ordinates of the vertices of T_k (see Figure 9), we have

$$A_0^k = a_1^k, \qquad A_1^k = a_2^k - a_1^k, \qquad A_2^k = a_4^k - a_1^k, \qquad A_3^k = a_3^k - a_2^k - a_4^k + a_1^k,$$
$$B_0^k = b_1^k, \qquad B_1^k = b_2^k - b_1^k, \qquad B_2^k = b_4^k - b_1^k, \qquad B_3^k = b_3^k - b_2^k - b_4^k + b_1^k.$$

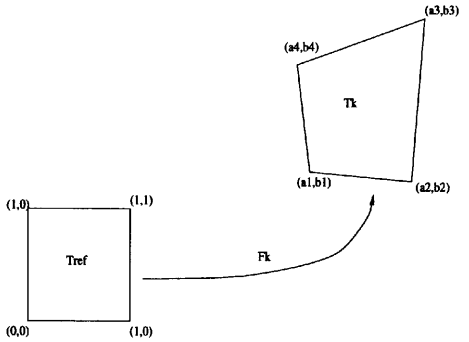

Figure 9. Quadrilateral T_k and reference unit square T_{ref}

The determinant of the Jacobian matrix of the transformation is

$$J^k(\xi, \eta) = A_1^k B_2^k - A_2^k B_1^k + (A_1^k B_3^k - A_3^k B_1^k)\xi + (A_3^k B_2^k - A_2^k B_3^k)\eta.$$

If $|T_k|$ denotes the area of T_k, let us remark that $J^k(\xi, \eta) = |T_k|$ as soon as T_k is parallelogram. The shape functions λ_i of the reference element are defined by

$$\lambda_1(\xi, \eta) = (1 - \xi)(1 - \eta), \qquad \lambda_2(\xi, \eta) = \xi(1 - \eta),$$
$$\lambda_3(\xi, \eta) = \xi\eta, \qquad \lambda_4(\xi, \eta) = (1 - \xi)\eta.$$

The shape functions ψ_i^k of T_k are defined by

$$\lambda_i = \psi_i^k \circ F^k.$$

One easily checks that

$$\int_{T_k} \frac{\partial \psi_i^k}{\partial x} \mathrm{d}x\mathrm{d}y = \int_{T_{\mathrm{ref}}} \left((B_2 + B_3\xi) \frac{\partial \lambda_i}{\lambda \xi} - (B_1 + B_3\eta) \frac{\partial \lambda_i}{\partial \eta} \right) \mathrm{d}\xi \mathrm{d}\eta, \tag{21}$$

$$\int_{T_k} \frac{\partial \psi_i^k}{\partial y} \mathrm{d}x\mathrm{d}y = \int_{T_{\mathrm{ref}}} \left(-(A_2 + A_3\xi) \frac{\partial \lambda_i}{\partial \xi} + (A_1 + A_3\eta) \frac{\partial \lambda_i}{\partial \eta} \right) \mathrm{d}\xi \mathrm{d}\eta. \tag{22}$$

I.2. Influence of the grid

We wonder whether the classical method could coincide with the method of projection presented in Section 4. In other words, we are looking for conditions which imply

$$\int_\Omega \Phi \operatorname{div} \mathbf{v}_j \mathrm{d}x\mathrm{d}y = \int_\Omega \Pi_h \Phi \operatorname{div} \mathbf{v}_j \mathrm{d}x\mathrm{d}y, \tag{23}$$

with $\mathbf{v}_j = (v_j, 0)$ or $(0, v_j)$ for all nodes j of the grid.

Proposition 1

If the elements of the mesh are identical rectangles whose sides are parallel to the co-ordinates axes and if $\Phi(x, y) = \Psi_1(x) + \Psi_2(y) + \beta(x, y)$, where Ψ_1 and Ψ_2 denote two arbitrary functions and β is an arbitrary bilinear application (or, more generally, if Φ satisfies property (15) of Section 4), then the classical method coincides with the projection method presented in Section 4.

Proof. Let us consider the four quadrilaterals T_k, $k = 1, \ldots, 4$, surrounding node j. In order to simplify the notation, we number them as in Figure 10. This allows us to write

$$v_j | T_k = \psi_k^k.$$

For the sake of simplicity we denote ψ_k^k by ψ_k, omitting the superscript k in the sequel.

Since we use the P0 finite element space for the pressure, $\Pi_h \Phi$ is constant over each T_k. By definition,

$$\Pi_h \Phi | T_k = \Phi_k = \frac{1}{|T_k|} \int_{T_{\mathrm{ref}}} \Phi \circ F_k(\xi, \eta) J \mathrm{d}\xi \mathrm{d}\eta.$$

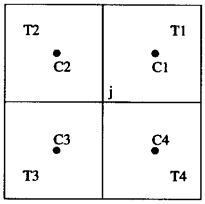

Figure 10. Four elements around node j

Taking $\mathbf{v}_j = (v_j, 0)$, we have

$$\int_\Omega \Pi_h \Phi \frac{\partial v_j}{\partial x} \mathrm{d}x\mathrm{d}y = \sum_{k=1}^{4} \Phi_k \int_{T_k} \frac{\partial \psi_k}{\partial x} \mathrm{d}x\mathrm{d}y$$
$$= \sum_{k=1}^{4} \Phi_k \int_{T_{\mathrm{ref}}} \left((B_2^k + B_3^k \xi) \frac{\partial \lambda_k}{\partial \xi} - (B_1^k + B_3^k \eta) \frac{\partial \lambda_k}{\partial \eta} \right) \mathrm{d}\xi\mathrm{d}\eta,$$
$$\int_\Omega \Phi \frac{\partial v_j}{\partial x} \mathrm{d}x\mathrm{d}y = \sum_{k=1}^{4} \int_{T_k} \Phi \frac{\partial \psi_k}{\partial x} \mathrm{d}x\mathrm{d}y$$
$$= \sum_{k=1}^{4} \int_{T_{\mathrm{ref}}} \Phi \circ F_k(\xi, \eta) \left((B_2^k + B_3^k \xi) \frac{\partial \lambda_k}{\partial \xi} - (B_1^k + B_3^k \eta) \frac{\partial \lambda_k}{\partial \eta} \right) \mathrm{d}\xi\mathrm{d}\eta.$$

Let us suppose that the quadrilaterals of the mesh are *parallelograms*. Then $A_3^k = 0$ and $B_3^k = 0$ for all k and $\Phi_k = \int_{T_{\mathrm{ref}}} \Phi \circ F_k(\xi, \eta) \mathrm{d}\xi\mathrm{d}\eta$. Doing the same calculus with $\mathbf{v}_j = (0, v_j)$, equation (23) is finally equivalent to

$$\begin{aligned} &\sum_{k=1}^{4} (-1)^k \int_{T_{\mathrm{ref}}} \Phi \circ F_k(\xi, \eta) [-A_1^k (\xi - \tfrac{1}{2}) + A_2^k (\eta - \tfrac{1}{2})] \mathrm{d}\xi\mathrm{d}\eta = 0, \\ &\sum_{k=1}^{4} (-1)^k \int_{T_{\mathrm{ref}}} \Phi \circ F_k(\xi, \eta) [-B_1^k (\xi - \tfrac{1}{2}) + B_2^k (\eta - \tfrac{1}{2})] \mathrm{d}\xi\mathrm{d}\eta = 0. \end{aligned} \tag{24}$$

Let us write these equalities on the parallelograms T_k:

$$\begin{aligned} &\sum_{k=1}^{4} \frac{(-1)^k}{|T_k|^2} \int_{T_k} \Phi(x, y) [2A_1^k A_2^k (y - y_{\mathrm{c}}^k) - (B_1^k A_2^k + A_1^k B_2^k)(x - x_{\mathrm{c}}^k)] \mathrm{d}x\mathrm{d}y = 0, \\ &\sum_{k=1}^{4} \frac{(-1)^k}{|T_k|^2} \int_{T_k} \Phi(x, y) [2B_1^k B_2^k (x - x_{\mathrm{c}}^k) - (B_1^k A_2^k + A_1^k B_2^k)(y - y_{\mathrm{c}}^k)] \mathrm{d}x\mathrm{d}y = 0, \end{aligned} \tag{25}$$

where $(x_{\mathrm{c}}^k, y_{\mathrm{c}}^k)$ are the co-ordinates of the centre of C_k of T_k.

Finally if the quadrilaterals are *rectangles* whose sides are parallel to the co-ordinate axes, we have $A_2^k = B_1^k = 0$ for all k and (25) becomes

$$\begin{aligned} &\sum_{k=1}^{4} \frac{(-1)^k}{|T_k|} \int_{T_k} \Phi(x, y)(x - x_{\mathrm{c}}^k) \mathrm{d}x\mathrm{d}y = 0, \\ &\sum_{k=1}^{4} \frac{(-1)^k}{|T_k|} \int_{T_k} \Phi(x, y)(y - y_{\mathrm{c}}^k) \mathrm{d}x\mathrm{d}y = 0. \end{aligned} \tag{26}$$

When all rectangles are identical, this relation is satisfied in particular by $\Phi(x, y) = \Psi_1(x) + \Psi_2(y) + \beta(x, y)$, where Ψ_1 and Ψ_2 are any functions and β is an arbitrary bilinear form.

Therefore, with forces $\mathbf{f}(x, y) = (f_1(x) + \alpha_1 y, f_2(y) + \alpha_2 x)$, formulations (10) and (13) are equivalent on meshes whose elements are identical and rectangular.

APPENDIX II

Our aim is to show that the projection method of Section 5 is more precise than the classical method in the case $\mathbf{f} = \nabla\Phi$.

We denote by $\mathbf{u}_h^c$ the velocity obtained with the classical method and $\mathbf{u}_h^p$ the velocity obtained by the projection method. We recall that the expected solution is $\mathbf{u} = 0$ and

$$\int_\Omega |\nabla \mathbf{u}_h^c|^2 \mathrm{d}x = -\frac{1}{\eta}\int_\Omega \Phi \operatorname{div} \mathbf{u}_h^c \mathrm{d}x, \tag{27}$$

whereas

$$\int_\Omega |\nabla \mathbf{u}_h^p|^2 \mathrm{d}x = \frac{1}{\eta}\int_\Omega (\mathbf{f} - \nabla\Phi_h)\cdot\mathbf{u}_h^p \mathrm{d}x = \frac{1}{\eta}\int_\Omega (\Phi_h - \Phi) \operatorname{div} \mathbf{u}_h^p \mathrm{d}x. \tag{28}$$

II.1. Notation

For any $h > 0$ we denote by $\mathscr{T}_h$ a regular 'triangulation' of $\bar{\Omega}$ of typical size h. We suppose here that any element $T \in \mathscr{T}_h$ is a quadrilateral, but it is not necessary.

As in Appendix I, T_{ref} is the reference unit square $[0, 1] \times [0, 1]$ and F_T is the bilinear mapping that maps T_{ref} onto any quadrilateral T. We denote by Q_k the space of all polynomials in the reference space of the form $\hat{q}(\xi, \eta) = \sum c_{ij}\xi^i\eta^j$, where the sum range over all integers i and j such that $0 \leqslant i, j \leqslant k$. We define $Q_k(T) = \{q = \hat{q} \circ F_T^{-1};\ \hat{q} \in Q_k\}$.

We introduce

$$\begin{aligned}
X_h &= \{\mathbf{v}_\in \mathscr{C}^0(\bar{\Omega})^2;\ \mathbf{v}_h|_T \in Q_k(T)^2, \quad \forall T \in \mathscr{T}_h\} \cap H_0^1(\Omega)^2,\\
M_h &= \{q_h \in L^2(\Omega);\ q_h|_T \in Q_l(T)^2, \quad \forall T \in \mathscr{T}_h\} \cap L_0^2(\Omega),\\
Y_h &= \{y \in \mathscr{C}^0(\bar{\Omega});\ y|_T \in Q_k(T), \quad \forall T \in \mathscr{T}_h\} \cap L_0^2(\Omega).
\end{aligned}$$

The space X_h is devoted to the velocity, M_h to the pressure and Y_h to the potential part of the force $\mathbf{f}$.

We provide $H^m(\Omega)$ with the seminorm

$$|v|_m = \left(\sum_{|\alpha|=m} \int_\Omega |D^\alpha v|^2 \mathrm{d}x\right)^{1/2}.$$

For $\mathbf{f} = \nabla\Phi$, with $\Phi \in H^{m+1}(\Omega) \cap L_0^2(\Omega)$, $m \geqslant 0$, we define $\Phi_h \in Y_h$ as the finite element solution of the Neumann problem

$$\begin{aligned}
-\Delta\Phi &= \operatorname{div}\mathbf{f} \quad \text{in } \Omega,\\
\frac{\partial\Phi}{\partial\mathbf{n}} &= \mathbf{f}\cdot\mathbf{n} \quad \text{on } \partial\Omega,
\end{aligned}$$

such that $\int_\Omega \Phi_h = 0$ (the condition on $\partial\Omega$ is formal when $m = 0$). More precisely, we have

$$\int_\Omega \nabla\Phi_h\cdot\nabla\psi_h \mathrm{d}x = \int_\Omega \mathbf{f}\cdot\nabla\psi_h \mathrm{d}x$$

for all $\psi_h \in Y_h$.

For $l \geqslant 0$ and $z \in L^2_0(\Omega)$ we recall that $\Pi_h z \in M_h$ is defined as

$$\Pi_h z|_T \in Q_l(T),$$
$$\int_T (\Pi_h z - z) q \mathrm{d}x = 0, \quad \forall q \in Q_l(T).$$

II.2. Error estimates

Proposition 2

We suppose that the force is gradient $\mathbf{f} = \nabla\Phi$ and we use the Q1/P0 pair of finite element space. Then, when the typical size h of the mesh tends to zero, the seminorm $|.|_1$ of the velocity calculated by the classical method tends to zero like h, whereas the velocity calculated by the projection method tends to zero like h^2.

Proof. First we recall the following approximation result (see e.g. Reference 2).

Lemma 1

Let $\Phi \in H^{m+1}(\Omega)$ for some m such that $0 \leqslant m \leqslant k$. If we define Φ_h as described in Section II.1,

$$|\Phi - \Phi_h|_1 \leqslant C_1 h^m |\Phi|_{m+1},$$

with a constant $C_1 > 0$ independent of h and Φ.

The following lemma is a straightforward application of a result of projection in $L^2(\Omega)$ presented in Reference 2.

Lemma 2

Let $z \in H^s(\Omega) \cap L^2_0(\Omega)$ for some s such that $0 \leqslant s \leqslant l+1$. The projection Π_h defined in Section II.1 satisfies

$$\|z - \Pi_h z\|_{L^2(\Omega)} \leqslant C_2 h^s |z|_s,$$

with a constant $C_2 > 0$ independent of h and z.

We restrict ourselves to the case $k = 1$, $l = 0$ corresponding to the pair Q1/P0. We choose $s = 1$ and $m = 1$ in the previous lemmas. In view of (27) we have

$$\begin{aligned} |\mathbf{u}_h^c|_1^2 &= -\frac{1}{\eta} \int_\Omega (\Phi - \Pi_h \Phi) \operatorname{div} \mathbf{u}_h^c \mathrm{d}x \\ &\leqslant \frac{1}{\eta} \|\Phi - \Pi_h \Phi\|_{L^2(\Omega)} \| \operatorname{div} \mathbf{u}_h^c \|_{L^2(\Omega)} \\ &\leqslant \frac{C_2}{\eta} h |\Phi|_1 \| \operatorname{div} \mathbf{u}_h^c \|_{L^2(\Omega)}. \end{aligned}$$

We deduce that

$$|\mathbf{u}_h^c|_1 \leqslant \frac{C_2}{\eta} |\Phi|_1 h. \tag{29}$$

On the other hand, from (28) the estimate of $|u_h^p|_1$ is

$$\begin{aligned}|\mathbf{u}_h^p|_1^2 &= -\frac{1}{\eta}\int_\Omega [(\Phi_h - \Phi) - \Pi_h(\Phi_h - \Phi)]\,\mathrm{div}\,\mathbf{u}_h^p \mathrm{d}x \\ &\leqslant \frac{1}{\eta}\|(\Phi_h - \Phi) - \Pi_h(\Phi_h - \Phi)\|_{L^2(\Omega)}\|\,\mathrm{div}\,\mathbf{u}_h^p\|_{L^2(\Omega)} \\ &\leqslant \frac{C_2}{\eta}h|\Phi_h - \Phi|_1\|\,\mathrm{div}\,\mathbf{u}_h^p\|_{L^2(\Omega)} \\ &\leqslant \frac{C_1 C_2}{\eta}h^2|\Phi|_2\|\,\mathrm{div}\,\mathbf{u}_h^p\|_{L^2(\Omega)}.\end{aligned}$$

Thus

$$|\mathbf{u}_h^p|_1 \leqslant \frac{C_1 C_2}{\eta}|\Phi|_2 h^2. \tag{30}$$

A comparison between (29) and (30) shows the improvement of the projection method in the case of $\mathbf{f} = \nabla\Phi$. These estimates may be better in some particular cases (see Table V).

REFERENCES

1. O. Besson, J. Bourgeois, P. A. Chevalier, J. Rappaz and R. Touzani, 'Numerical modelling of electromagnetic casting processes', *J. Comput. Phys.*, **92**, 482–507 (1991).
2. V. Girault and P.-A. Raviart, *Finite Element Methods for Navier– Stokes Equations*, Springer, New York, 1986.
3. M. D. Gunzburger, *Finite Element Methods for Viscous Incompressible Flows: A Guide to Theory*, *Practice*, *and Algorithms*, Academic, New York, 1989.
4. J. M. Leone and P. M. Gresho, 'Another attempt to overcome the bent element blues', *Proc. 5th Int. Conf. on Finite Element Methods in Water Resources*, Burlington, 1984, Springer, New York, 1984, pp. 667–683.

